Summer 7-31-2017

# Molecular Dynamics Modeling and Simulation of Bitumen Chemical Aging

Farshad Fallah
*University of Nebraska - Lincoln*, farshad.fallah@huskers.unl.edu

# MOLECULAR DYNAMICS MODELING AND SIMULATION OF BITUMEN CHEMICAL AGING

by

Farshad Fallah

A THESIS

Presented to the Faculty of

The Graduate College at the University of Nebraska

In Partial Fulfillment of Requirements

For the Degree of Master of Science

Major: Civil Engineering

Under the Supervision of Professor Yong-Rak Kim

Lincoln, Nebraska

July 2017

# MOLECULAR DYNAMICS MODELING AND SIMULATION OF BITUMEN CHEMICAL AGING

Farshad Fallah, M.S.

University of Nebraska, 2017

Advisor: Yong-Rak Kim

Chemical aging of asphalt binder leads to significant changes in its mechanical and rheological properties, resulting in poor pavement behavior and distress. Various laboratory methods have been used to simulate asphalt aging during the service life of the pavement. However, controversy exists regarding the capability of these methods to predict field aging, as various factors interact with the pavement during service and the mechanism behind aging is not fully understood. The two main outcomes of chemical aging are oxidation of asphalt molecules, and change in asphalt SARA (saturate, aromatic, resin, and asphaltene) fractions. Reaction of oxygen with asphalt components forms polar viscosity-building molecules, while the change in SARA fractions upsets the balance in asphalt, giving it brittle properties. As both these factors affect the binder at the molecular level, molecular dynamic (MD) simulations can provide core insights into understanding the fundamentals of asphalt aging. This study used MD simulation to investigate the effect of each aging process on the properties of asphalt binder. In that respect, a representative model of virgin binder and eight different models of aged binder were built, including models for laboratory- and field-aged binder. Properties such as density, bulk modulus, glass transition temperature, and viscosity from different MD models were compared to distinguish between the effect of each aging mechanism on

binder properties. The results showed that both aging mechanisms lead to an increase in density, bulk modulus, and viscosity of the binder. The SARA fractions of laboratory-aged binder were found to affect bulk modulus and viscosity more dramatically compared to field aged binder. However, when the oxygen content of models was considered, field-aged binder showed a larger increase in bulk modulus and viscosity compared to laboratory-aged binder. This indicates that the dominant mechanism from laboratory aging process is upset in SARA fractions, while oxidation of molecules might be a more dominant mechanism for field-aged binder. No statistically significant difference was observed between the glass transition temperature values for virgin and aged binder.

# ACKNOWLEDGMENTS

I would like to express my gratitude to my advisor Dr. Yong-Rak Kim for his support during my studies and inspiring me to strive for excellence. Dr. Kim taught me to think critically, and helped me to grow as an independent thinker. I would also like to thank my thesis committee members Dr. Mehrdad Negahban and Dr. Jiong Hu as well as my friends for their help and support during my studies.

# Table of Contents

# List of Figures

# List of Tables

# CHAPTER 1
# INTRODUCTION

## 1.1 Problem statement

Asphalt binder is a petroleum product used widely in pavement construction. It is a multi-component material composed of close to a million type of compounds, ranging from large polar to small nonpolar molecules. The interaction between these molecules determines the macroscale properties of asphalt, which are often hard to characterize and predict.

During pavement construction and service life, asphalt binder interacts with different environmental factors and undergoes chemical changes that alter its properties. This process is known as chemical aging, and leads to reduced ductility and increased brittleness of the binder, making it more susceptible to distresses such as cracking. The mechanism behind chemical aging is not fully understood. Various methods have been used to characterize aging, ranging from analysis of different asphalt fractions to elemental analysis and Fourier transform infrared spectroscopy. Currently, the two major indicators of chemical aging are believed to be the upset in the balance of constituent asphalt fractions, and the oxidation of asphalt molecules:

- Change in the balance of various chemical classes within asphalt alters the properties of binder, making it develop undesirable properties
- Oxidation of asphalt molecules, also called oxidative aging, leads to hardening of asphalt and makes it more susceptible to cracking

Both these processes affect the asphalt at the molecular level, and both happen during laboratory and field aging of binder. Laboratory scale testing is not capable of differentiating the effect of each factor, and can only capture the combined effect on binder properties.

## 1.2 **Research objectives and scope**

This study aims to investigate the effect of different aging processes on asphalt binder properties. Since aging mechanisms affect the asphalt at the molecular scale, investigation of the change in macroscale properties using molecular dynamic simulation can provide core insights into the process of chemical aging. In this regard, different models of aged binder were simulated and compared to virgin binder model to understand how change in the molecular level of binder due to aging affects macroscale properties of asphalt. In addition to the virgin control binder, four models with increasing degrees of oxidation were simulated to investigate the effect of asphalt oxidation on binder properties. Two aged binder models were built with no oxidation, using asphalt fractions obtained from analysis of laboratory-aged binder and field-aged binder, to observe the effect of fractions on asphalt properties. Finally, two aged binder models considering both oxidation and change in fractions were built to investigate cumulative effects of these factors on asphalt behavior. Comparison of the properties of different models are expected to provide insights into the mechanism and outcome of chemical aging.

## 1.3 **Organization of thesis**

This thesis consists of five chapters. Following this introduction, chapter 2 provides a review of studies involving asphalt binder, focusing on aspects related to asphalt composition, aging, and molecular dynamics studies on asphalt. In chapter 3, the methodology used for the molecular dynamic simulation is presented. Information regarding model characteristics and a brief introduction to molecular dynamic simulations is provided, followed by the methods used to calculate binder properties. Chapter 4 presents and discusses the results obtained from this study, comparing the properties of different binder models. Finally, chapter 5 summarizes the main findings of this study and provides recommendation for further research in this field.

# CHAPTER 2
# LITERATURE REVIEW

## 2.1 General information

Asphalt is a black adhesive material present in nature, and is mainly obtained as a byproduct of crude petroleum distillation. It is highly viscous and close to solid at ambient temperature, with a glass transition temperature ranging from -40 °C to 5 °C based on the crude petroleum origin and manufacturing process (Claudy et al. 1992). It has been used since ancient times, with main applications in road construction and waterproofing.

The elemental composition of asphalt varies based on the crude petroleum source. Since asphalt molecules are predominantly hydrocarbons, it mainly consists of carbon (82-88% by weight) and hydrogen atoms (8-12%). It also contains heteroatoms such as sulfur (0-6%), Nitrogen (0-1%), and oxygen (0-1.5%), and trace amounts of minerals such as vanadium, nickel, iron and magnesium, that are present in the form of inorganic salts and oxides. (Branthaver et al. 1993, Mortazavi and Moulthrop 1993, Read and Whiteoak 2003).

Asphalt is believed to consist of close to a million different organic compounds, without a single pure compound dominating its property (Wiehe et al. 1996). This complexity makes it extremely difficult to characterize the chemical structure of its constituents. The mechanical, physical and chemical properties of asphalt are governed by the configuration and interaction of the polar, nonpolar, small, and large molecules

constituting it (Petersen et al 1994). These numerous molecules assemble into systems for which the structure is not fully understood.

## 2.2 **Asphalt components**

Asphalt has an extremely complex chemical composition, and thus a complete analysis and correlation of properties with the large quantity of data would be highly laborious and impractical. However, it is possible to characterize asphalt chemically by its hydrocarbon class compositions, namely saturates (S), aromatics (A), resins (R), and asphaltenes (A). Also called SARA, these fractions can be separated based on the selective adsorption-desorption method proposed by Corbett (1969), according to their size and solubility in polar, non-polar or aromatic solvents.

### 2.2.1 Asphaltenes

Asphaltenes are the largest and most polar components of asphalt, making the largest contribution to its viscosity, and strongly affecting its rheological and mechanical properties (Mullins 2010). They comprise 5-25% of asphalt by weight, and are defined as the fraction of asphalt that is insoluble in light alkanes of n-pentane, n-hexane or n-heptane, but is soluble in aromatic solvents such as benzene or toluene. Asphaltenes present a black powder at room temperature, and do not show any thermal transition in temperatures up to 200°C (Lesueur 2009).

Although considerable effort has been devoted to the study of chemical and physical properties of asphaltenes, their molecular structure is still debated, their molecular weight being a controversy for decades (Mullins 2010). They are generally thought to be polycyclic aromatic compounds with alkyl side chains and heteroatoms (Li and

Greenfield 2013). Numerous molecular models have been put forward for asphaltenes, which can be categorized into island and archipelago types, both supported by experimental studies. Island models support the idea of asphaltene molecules composed by one medium-size fused aromatic ring (FAR) region with aliphatic chains. Archipelago models propose asphaltene molecules where many FAR regions are connected by short aliphatic carbon chains (Martin Martinez 2015).

Asphaltenes are known to form clusters at the nanoscale. This is caused by the p-p interactions between asphaltene molecules, due to delocalization of p electrons in the FAR region of these molecules. Debates arise also in regards to the supra-molecular arrangement, and both colloidal distribution of molecular aggregates and molecularly disperse models have been reported. Understanding the implications of different geometries and sizes on the stability of the molecules is essential to understand their supra-molecular arrangement (Martin Martinez 2015). A review by Lesueur (2009) on the structure of asphalt noted that asphalt possesses a colloidal structure with asphaltenes forming micelles surrounded by resins and entrapped in a solution of saturates and aromatics.

### 2.2.2 Saturates

Saturates consist of aliphatic chains with branched and cyclic alkanes. They are light and non-polar molecules, and constitute 5 to 15% of a paving-grade asphalt (Corbett 1969). Because of the low chemical reactivity of the saturates fraction, it is highly resistant to ambient air oxidation. A study of a group of asphalts from 18-year-old Michigan state test roads showed no measurable loss of the saturates fraction due to oxidation during the 18-year service period (Petersen 2009).

### 2.2.3 Aromatics

Aromatics, also referred to as naphthene aromatics, are low molecular weight molecules composed of non-aromatic rings and non-polar carbon chains. They have high dissolving ability for higher molecular weight hydrocarbons and form a yellow to red liquid at room temperature (Corbett 1969). Together with resins, they are the most abundant component in asphalt, constituting 30-45% of asphalt by weight. They are more viscous than saturates at the same temperature, but less viscous than resins (Claudy et al. 1992).

### 2.2.4 Reins

Resins, also called polar aromatics, are hydrocarbons containing nonpolar paraffinic groups and hetero atoms such as oxygen, sulfur, and nitrogen. The presence of heteroatoms makes them much more polar than saturates and aromatics. Resins form a black solid at room temperature (Corbett 1969).

## 2.3 **Asphalt aging**

Chemical aging of asphalt results in hardening and brittleness in asphalt, increasing the probability of cracking in pavements. It is an irreversible change that involves oxidation and polymerization of the molecules present in asphalt binder. Aging typically occurs at two stages. The first stage happens during mixing and laying of asphalt concrete and is called short term aging. Asphalt is usually heated to 135-160 ºC to achieve sufficient workability for mixing and construction. In this temperature, the low molecular weight fraction of asphalt evaporates, and the ratio of viscosity building fractions increases, leading to an increase in binder viscosity (Bell 1989). This stage of aging is usually simulated in laboratories by the Rolling Thin Film Oven (RTFO) technique. The second stage of binder aging occurs over the service life of pavement, and is called long term

aging. This stage is usually simulated using Pressure Aging Vessel (PAV) test. However, some researchers have reported that this method may not reliably simulate the aging that occurs in field under service conditions (Boysen et al. 2015, and Qin 2014). Aging of asphalt is usually characterized by the change in SARA fractions of asphalt, as well as oxidation indicators such as oxygen content of the system and carbonyl and sulfoxide indices in Fourier Transform Infrared Spectroscopy (FTIR) analysis.

### 2.3.1 Change in SARA fractions

During the aging process, there is an increase in resin and asphaltene fractions of asphalt, and a decrease in aromatic content. The aromatic fraction is believed to convert to resin fraction, and the resins are believed to convert to asphaltenes (NCAT 2014). In the case of saturates, there is a general agreement that no change occurs due to their low reactivity (Peterson 1993).

### 2.3.2 Oxidative aging

When asphalt in pavement is exposed to atmospheric oxygen, it oxidizes and forms polar functional groups that alter the rheological properties of binder (Petersen 1984). Oxidative aging of asphalt can be narrowed down to the reactions of certain types of functional groups with oxygen, as many different asphalt molecules share these chemical functional groups (Petersen 1986).

Ketone and sulfoxide functional groups are identified as the major products of asphalt oxidative aging (Peterson and Glaser 2011). Benzylic carbon is the carbon atom adjacent to an aromatic ring system, and is the most sensitive hydrocarbon part in asphalt (Robertson 1991). Ketones are formed when the hydrogen atom attached to benzylic

carbon atoms is replaced by oxygen. Sulfoxides are a chemical functional group containing a sulfinyl functional group, S=O, attached to two carbon atoms. Sulfoxides formed at sulfur atoms in asphalt are also one of the major products of oxidative aging. Figure 2.1 illustrates the formation of the major outcomes of oxidative aging.

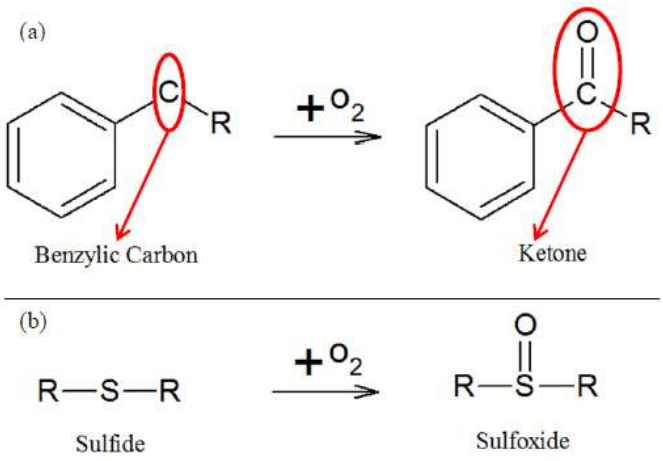


Figure 2.1 Formation of ketone and sulfoxide, from Pan and Tarefder (2016)

The oxidation reactions in asphalt were also investigated using ab initio quantum chemistry calculations, with X-ray photoelectron spectroscopy (XPS) used as validation for computational models (Pan et al. 2012 a, b). They concluded that ketones and sulfoxides are the major oxidation products formed in oxidative aging, while amine groups (nitrogen compounds) do not show contribution to asphalt hardening.

Direct measurement of ketone formation in oxidized fractions of asphalt by Petersen et al. (1974) ranked the relative reactivity of saturates, naphthene aromatics, polar aromatics, and asphaltenes fractions with atmospheric oxygen as 1:7:32:40, respectively. The production of ketones in asphalt has practical significance because it has been shown that the amount of ketones formed is linearly related to the increase in log viscosity of the asphalt—the viscosity being an important performance-related property (Peterson 2009).

## 2.4 **Molecular models of asphalt**

To do molecular dynamic simulations of a complex and multicomponent material such as asphalt, model molecules should be used to represent the large number of different compounds within asphalt. Different molecular models of asphalt have been proposed and used for simulation in the past, with initial models considering one average molecule to represent asphalt binder, and newer models proposing higher number of molecule to represent different fractions of asphalt binder.

Jenning et al. (1993) used nuclear magnetic resonance (NMR) spectroscopy on eight core asphalt binders to obtain data such as the amount of aromatic carbons and arrangement of the aliphatic portion in average molecules. Using this data, they proposed average molecular structures for asphalt binder. Murgich et al. (1996) used average asphaltene and resin molecular models to investigate asphaltene aggregation and found that the driving interaction in the micelle formation is the attraction between aromatic planes of asphaltene and resin molecules. Artok et al. (1999) used several experiments to study the structural characteristics of a pentane-insoluble asphaltene isolated from the vacuum residue of an Arabian crude mixture, and found that the average size of aromatic fused ring systems was 4-5 for the sample. Groenzin et al. (2000) used Fluorescence depolarization measurements to determine the size of coal and petroleum asphaltenes, and recommended more asphaltene model structures. Rogel et al. (2003) built average asphaltene structures based on different types of Venezuelan crude oil and estimated their density using molecule dynamic simulations. They also studied the effect of different structural factors such as the size of aromatic rings on calculated densities of asphaltenes. Takanohashi et al. (2003) proposed 3 asphaltene molecules based on experiments on

asphaltene obtained from the vacuum residue of Khafji crude oil and investigated the changes induced in molecule aggregation due to heating via molecular dynamics. Siskin et al (2006) used NMR, X ray photoelectron spectroscopy (XPS) and elemental abundance tests to characterize the average chemical structure of several asphaltenes.

Zhang and Greenfield (2007) developed an asphalt model for MD simulation using 2 asphaltene molecules, 1 saturate molecule, and 1 aromatic molecule. They used n-docosane (n-$C_{22}H_{46}$) to represent the saturate fraction and 1,7-Dimethylnaphthalene to represent the aromatic fraction. Two asphaltene molecules were used, one with a moderate-size aromatic core with small branches, taken from Artok et al. (1999), and one with smaller aromatic core and longer alkane side branches, taken from discussions by Groenzin and Mullins (2000) of their fluorescence depolarization studies. The molecular structure of all fractions is shown in Fig 2.2.

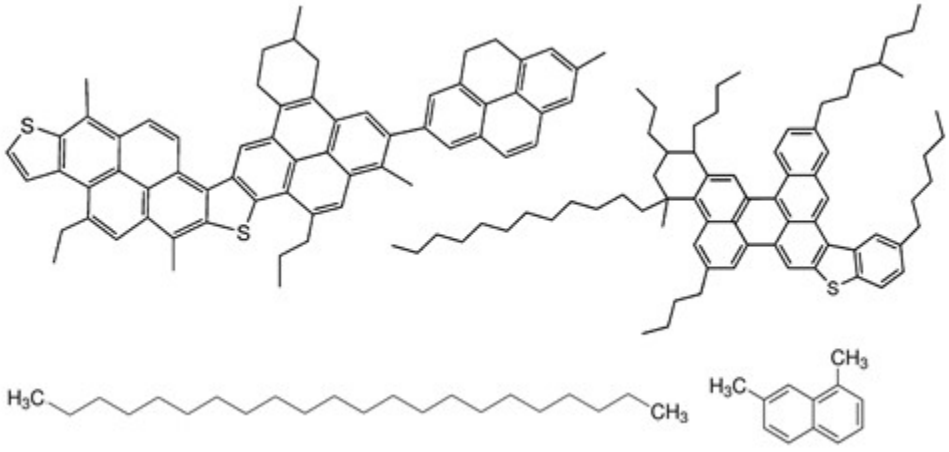


Figure.2.2 Molecules used by Zhang and Greefield (2007)

Hansen et al. (2013) proposed a four-component molecular model employing a single molecule for each saturated hydrocarbon, resinous oil, resin and asphaltene types. Using a united-atom model and graphic-processor-unit based software enabled the simulation of asphalt in time spans in the order of microseconds, which is significantly larger than the time spans achievable using all-atom models. High-temperature dynamics and relaxations were analyzed for each molecule type, and the model shear viscosity and shear modulus values were calculated.

Li and Greenfield (2014) proposed a 12-component model asphalt system to represent the AAA-1, AAK-1, and AAM-1 asphalts of the Strategic Highway Research Program (SHRP). They used squalane and hopane to represent the saturate fraction of asphalt, based on experimental research on the saturate fraction of SHRP asphalts. Two molecules, namely dioctyl-cyclohexane-naphthalene (DOCHN) and perhydrophenanthrene-naphthalene (PHPN), were used to represent the aromatic fraction. Five molecules were used for the resin fraction, with molecules named as benzobisbenzothiophene, pyridinohopane, quinolinohopane, trimethylbenzene-oxane, and thio-isorenieratane. The molecular structures are proposed based primarily on geochemistry literature on the analysis of petroleum found in sedimentary rock deposits. Three molecules are used to represent the asphaltene fraction, each including a different heteroatom. The asphaltene molecules were slightly modified versions of the molecules proposed by Mullin (2010) based on the most probable molecular weight within island architecture. These molecules are named as asphaltene-phenol, asphaltene-pyrrole, and asphaltene-thiophene. Characteristics of the models were matched to elemental and SARA analysis results specific to each binder. They achieved densities that were closer to

experimental values compared to their previous 3 component model for asphalt. However, they were not able to match the aliphatic carbon and sulfur content of models with experimental values, as most of the molecules had high aromatic to aliphatic carbon ratio and no sulfur atoms. Figure 2.3 shows the proposed molecules for each asphalt fraction.

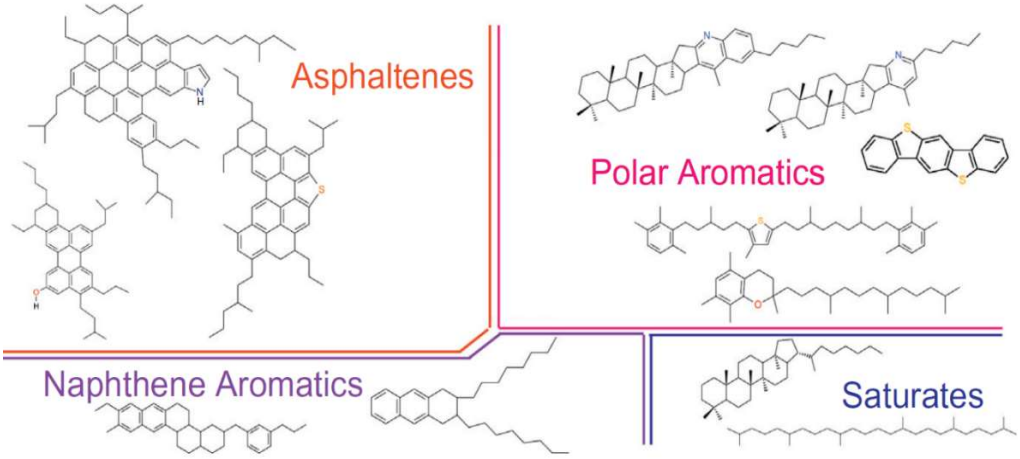


Figure 2.3 Molecules used to represent asphalt. Taken from Li and Greenfield (2013) with modification

Martin-Martinez et al. (2015) proposed modifications to the asphaltenes used by Zhang and Greenfield (2007) and Li and Greenfield (2014) which leads to lower internal energies and higher probability of occurrence in asphalt. Based on Clar sextet theory and density functional theory, they optimized the distribution of p electrons in the polycyclic aromatic core and minimized geometrical strain within the molecule. The resulting asphaltene molecules are shown in figure 2.4.

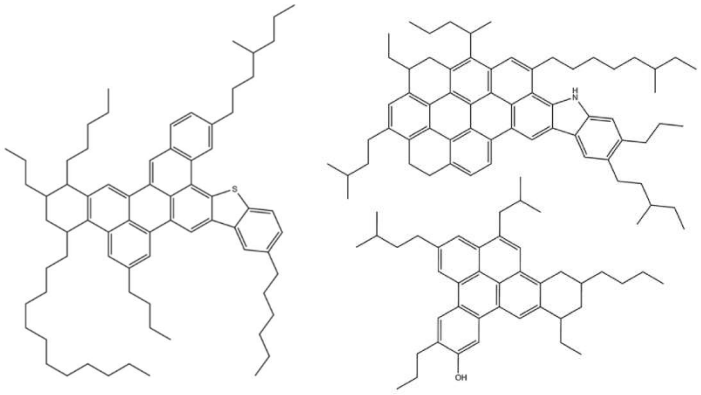

Figure 2.4 Asphaltene molecules proposed by Martin-Martinez et al. (2015)

## 2.5 **Research on asphalt using MD**

A comprehensive review by Greenfield (2011) on molecular simulation of asphaltenes and asphalt binder indicated that the molecular composition of asphaltenes plays an important role in their agglomeration. Continental and archipelago asphaltenes show different packing tendencies, while alkyl side chains bonded to aromatic rings interfere with multiple ring stacking layers. Diversity of molecular structures were also seen to be important for achieving a well-packed structure and avoiding unphysical concepts such as bent aromatic rings. Lastly, quantum mechanics simulations were seen to support continental asphaltene models.

Bhasin et al. (2010) investigated self-healing phenomena in asphalt binders using molecular dynamics. Two systems of molecules were used, one with average asphalt molecules for six different types of asphalt binder, and one with an ensemble of three types of molecules representing different fractions of binder. Both systems showed higher diffusivity rates for higher $CH_2/CH_3$ ratio and lower methylene plus methyl hydrogen to carbon ratio (MMHC), which are directly proportional to chain length and inversely proportional to branching, respectively. The findings demonstrated a good correlation

between chain length and the self-diffusivity of molecules at a crack interface, which influences the rate of intrinsic healing in asphalt binders.

Khabaz and Khare (2015) investigated the glass transition and molecular mobility for neat and styrene−butadiene rubber (SBR) modified asphalt using molecular dynamic simulations. Radial distribution function showed increased aggregation of asphaltenes after adding SBR molecule, and the mobility of constituent molecules were reduced. The volume-temperature behavior of the systems exhibited a glass transition phenomena, but the glass transition temperature was not seen to be different for neat and SBR modified asphalt within statistical uncertainties.

Xu and Wang (2016) studied cohesive and adhesive properties of asphalt with molecular dynamics simulation and compared them with experimental data. Two representative asphalt models and two types of aggregate minerals were used, and properties such as solubility parameters, cohesive energy density and surface free energy were computed. The results showed that the adhesion bonding between asphalt and aggregate is largely dependent on the type of aggregate mineral (silica or calcite).

Wang et al. (2017) used molecular dynamics to simulate asphalt-aggregate interface adhesion strength in the presence of moisture. The stress-separation curve under tension obtained in the simulation resembled the failure behavior at macroscopic scale, with an initial linear part followed by a gradually decaying process. It was seen that the presence of water molecules at the asphalt-quartz interface significantly reduces the interface adhesion strength, with higher moisture and temperature inversely affecting the adhesion strength.

## 2.6 MD studies of aging

Lemarchand et al. (2013) investigated the effect of chemical aging on binder using a united-atom model. Asphalt aging was modeled by converting to two resin molecules to an asphaltene molecule. The stress autocorrelation function, fluid structure, rotational dynamics, and diffusivity of each molecule was determined. It was found that aging causes a significant dynamics slowdown, which is correlated to the aggregation of asphaltene molecules in larger and dynamically slower nanoaggregates.

Yao et al. (2016) investigated the adhesion energies between asphalt-aggregate and water-aggregate systems and found that water tends to adhere to aggregates rather than asphalt. They also found that the asphalt-aggregate system with carboxylic acid group had higher adhesion energies than those of the control system, suggesting that the improvement in adhesion energy of aged binder leads to moisture damage resistance in asphalt mixtures.

Xu et al. (2016) investigated the adhesive bonding between asphalt binder and silicate minerals in aggregate by using the silicate tip of an atomic force microscope. They used molecular dynamic simulations and atomic force microscopy (AFM) test to characterize the bonding for virgin, short-term aged and long-term aged binders. The number of asphalt molecules were adjusted to conform to the experimental measurements of SARA fractions of virgin and aged binders. They demonstrated that molecules with a higher atomic density and planar structure, such as asphaltene molecules, can provide greater adhesive strength than other molecules. They also proposed that the colloidal structural behavior of asphalt has a large influence on the adhesion behavior between asphalt and

silicon, as short term aged binder exhibited higher adhesion performance despite lower amount of asphaltene molecules.

Pan and Tarefder (2016) investigated the change in properties of asphalt binder due to oxidation aging. They introduced carbonyl and sulfoxide functional groups to the 12-component model of Li and Greenfield (2013) to represent aged binder. They found that oxidation of asphalt molecules leads to higher density, bulk modulus, and viscosity values. Compressive and tensile tests of unoxidized and oxidized asphalts showed that oxidized asphalt deforms slower and to a less extent compared to unoxidized asphalt.

Xu and Wang (2017) similarly studied the effect of oxidative aging on asphalt binder properties using the 12-component model of Li and Greenfield (2013). Aging of the model was achieved by introducing ketone and sulfoxide functional groups into virgin asphalt. They showed that density, viscosity, and cohesive energy density increases with aging, while surface free energy decreases. They proposed that aging weakens the nano-aggregation behavior of asphaltenes and reduces the translational mobility of asphalt molecules. Activation energy barrier for self-healing was found to be higher for aged asphalt compared to virgin asphalt, and the degradation of work of adhesion was more significant in aged binder after addition of water molecules, compared to virgin binder.

Ding et al. (2016) investigated the diffusion between virgin and reclaimed asphalt binder via concentration profiles across the simulation domain. A three-component asphalt model was used and aged binder was simulated by increasing the asphaltene fraction content. The effect of adding rejuvenator to mixture was also investigated. It was found

that adding rejuvenator to aged binder before mixing with virgin binder increased inter-diffusion rate more than adding it virgin binder.

# CHAPTER 3
# RESEARCH METHODOLOGY

## 3.1 Asphalt molecules before oxidation

Due to the realistic density values obtain by Li and Greenfield (2013) and the lower internal energies of asphaltenes presented by Martin-Martinez et al. (2015), the models proposed in those two studies were used to build the asphalt models without additional oxygen. The polar aromatic, naphthene aromatic, and saturate molecules were taken from Li and Greenfield (2013), and the asphaltene molecules are taken from Martin-Martinez et al. (2015). Figures 3.1 to 3.4 show the molecular structure of asphaltene, saturate, polar aromatic, and naphthene aromatic molecules used, respectively.

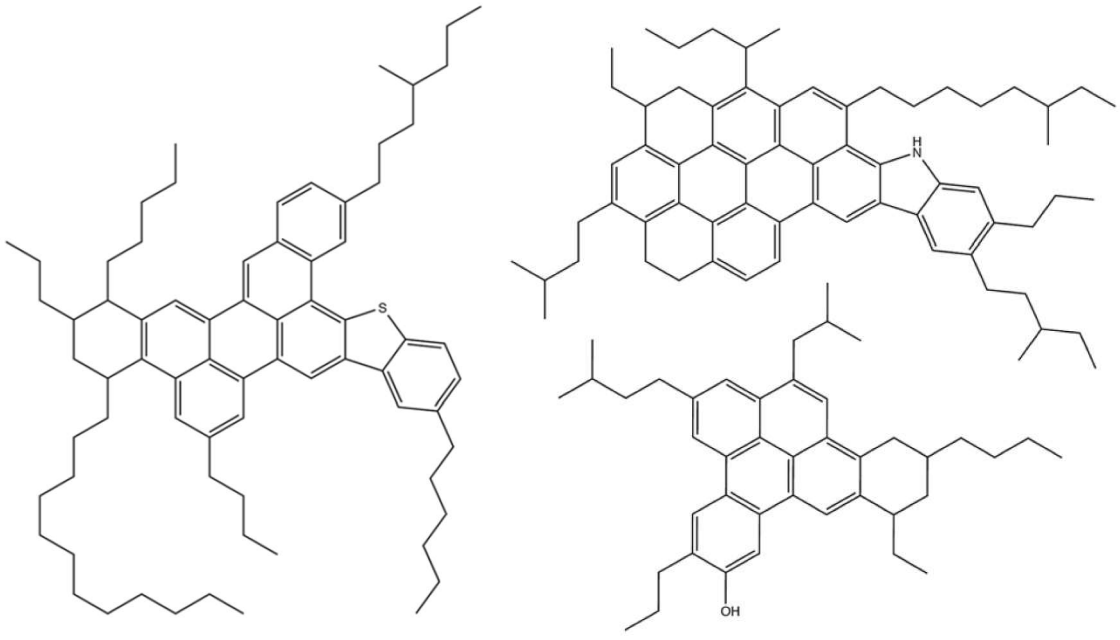


Figure 3.1 Asphaltene molecules used in this study. From Martin-Martinez et al. (2015)

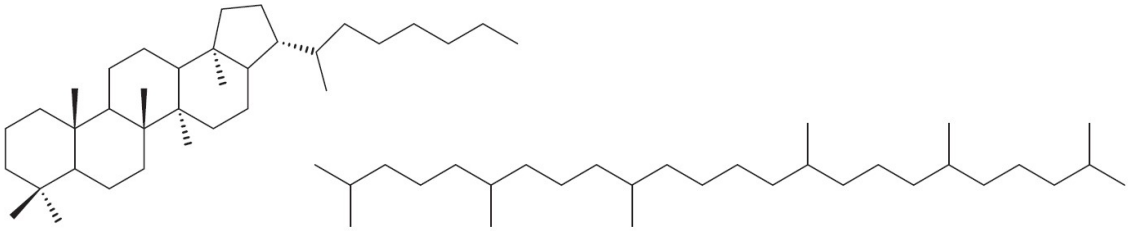

Figure 3.2 Saturates molecules used in the asphalt model, from Li and Greenfield (2013)

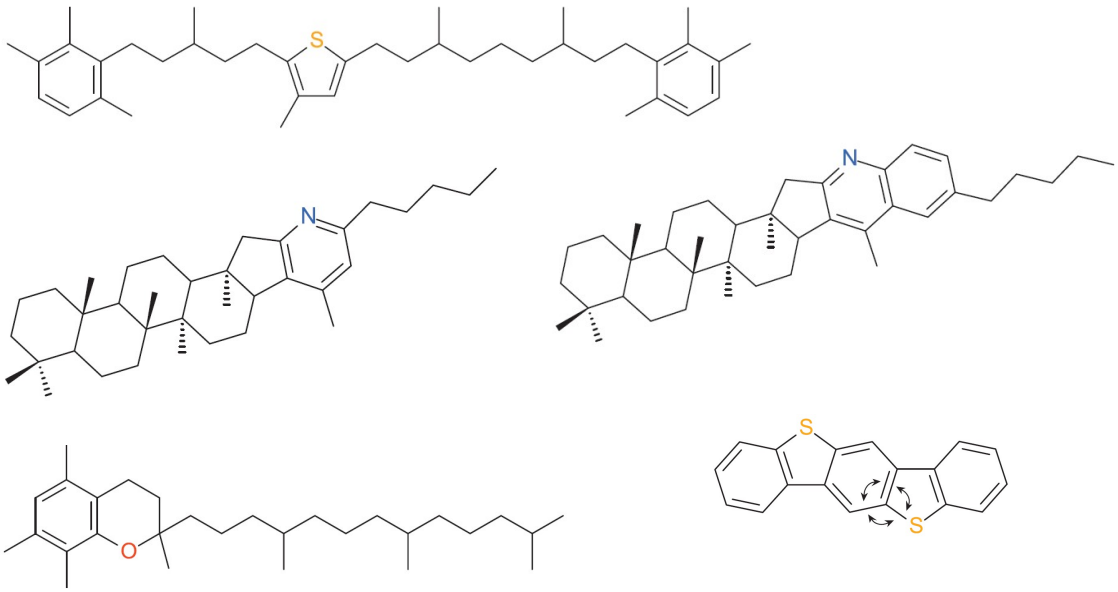


Figure 3.3 Molecules used to represent resin fraction, from Li and Greenfield (2013)

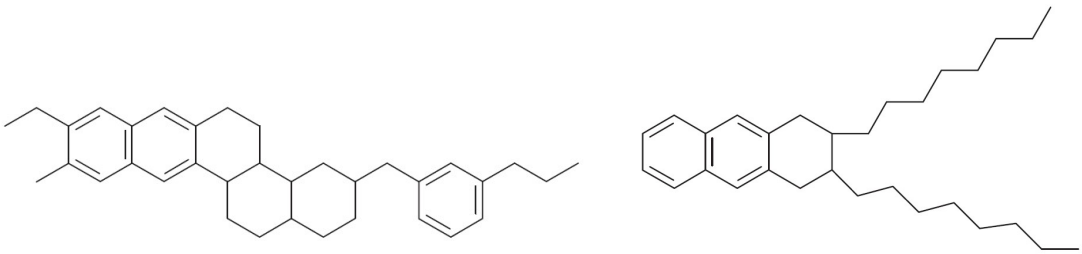

Figure 3.4 Naphthene aromatic molecules, from Li and Greenfield (2013)

## 3.2 **Asphalt molecules after oxidation**

Oxidized asphalt molecules were developed by adding oxygen atoms to sensitive chemical functional groups of unoxidized asphalt molecules. As previously stated, ketones formed at benzylic carbon atoms adjacent to aromatic ring systems, and sulfoxides formed at sulfide functional groups are the two major products of oxidative aging. Therefore, based on the oxygen content necessary for each model, different numbers of oxygen atoms were added to the sensitive functional groups, prioritizing asphaltenes molecules over resins, and resins over naphthene aromatics. The saturates have no change due to oxidation as they do not contain any sensitive functional groups. Figures 3.5 and 3.6 show a schematic representation of the oxidation process, and an asphaltene molecule with different oxidation degrees, respectively.

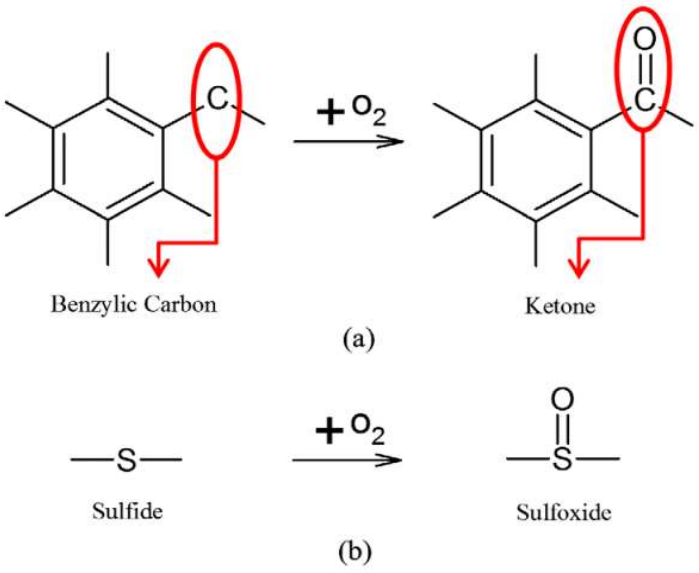


Figure 3.5 Oxidation of sensitive functional groups, from Pan and Tarefder (2016)

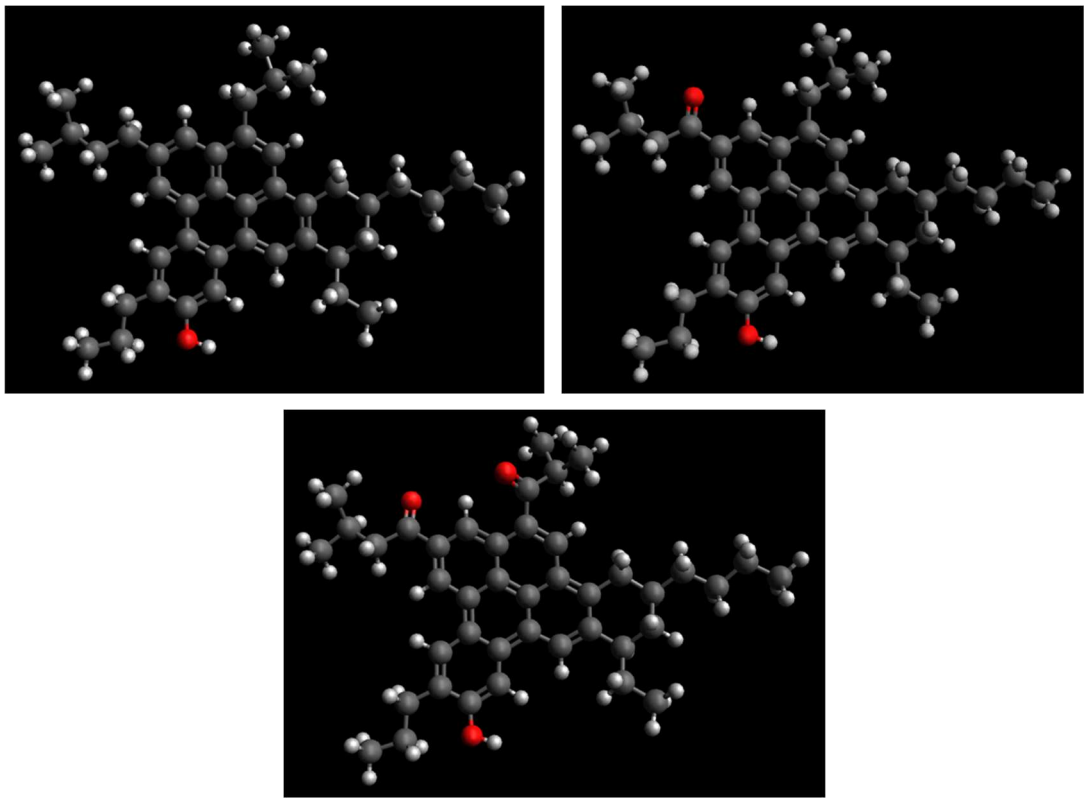

Figure 3.6 An asphaltene molecule with zero, one, and two added oxygen atoms

## 3.3 Asphalt models

To make realistic molecular dynamic models of virgin and aged binder, the results of SARA and elemental analysis of virgin binder, pressure aging vessel (PAV) aged binder, and reclaimed asphalt binder (RAB) were used to build the MD asphalt models. All binders have a PG grading of 64-28, and were obtained from the same source. Table 3.1 shows the SARA mass fractions and oxygen content of each binder. Although heteroatoms such as sulfur and nitrogen play an important role in the properties of binder, this study only considered the effect of oxygen to exclusively examine the effects of oxygen on binder properties with aging.

Table 3.2 SARA mass fractions and oxygen content of different binder specimens

| Virgin binder | | PAV aged binder | | RAB | |
|---|---|---|---|---|---|
| Component | % Content | Component | % Content | Component | % Content |
| Saturate | 6.4 | Saturate | 6.3 | Saturate | 6 |
| Aromatics | 48.6 | Aromatics | 38.3 | Aromatics | 40.4 |
| Resin | 28.5 | Resin | 30.6 | Resin | 33.8 |
| Asphaltenes | 16.5 | Asphaltenes | 24.8 | Asphaltenes | 19.8 |
| Oxygen | 0.9 | Oxygen | 1.4 | Oxygen | 2.6 |

A total of nine MD models were built in this study, each with different SARA mass fractions and/or oxygen content. The models were built by manually manipulating the number of oxygen atoms and different molecules in the system, until a good match between the model and experimental values of SARA mass fractions and oxygen content was obtained. Table 3.2 shows the comparison between the model and experimental values of SARA mass fractions and oxygen for virgin and PAV aged binders. Table 3.3 shows the number of each molecule and oxygen atoms added for each asphalt model.

Table 3.1 Model and experiment SARA fractions and oxygen content for a) virgin and b) PAV aged binder

a)

| Component | Target % content | Model % content |
|---|---|---|
| Saturate | 6.4 | 6.4 |
| Aromatics | 48.6 | 48.7 |
| Resin | 28.5 | 28.3 |
| Asphaltenes | 16.5 | 16.6 |
| Oxygen | 0.90 | 0.91 |

b)

| Component | Target % content | Model % content |
|---|---|---|
| Saturate | 6.6 | 6.3 |
| Aromatics | 38.3 | 37.9 |
| Resin | 30.6 | 30.7 |
| Asphaltenes | 24.8 | 24.7 |
| Oxygen | 1.38 | 1.38 |

To investigate the effect of increased oxygen content on the properties of asphalt binder, four models in addition to the control virgin binder model were built with increasing oxygen content but similar SARA mass fractions to those of the control binder. The elemental analysis of virgin binder showed an oxygen content of 0.9%, as shown in Table 3.2.

Table 3.3 Number of molecules and added oxygen atoms for virgin and PAV aged binder models

| Asphalt fraction | Molecule | Number in Virgin binder model | Number in PAV aged binder model | Oxygen atoms |
|---|---|---|---|---|
| Asphaltenes | Asphaltene 1 | 2 | 2 | +2 |
| | Asphaltene 2 | 1 | 3 | +1 |
| | Asphaltene 3 | 5 | 6 | |
| Aromatics | PHPN | 19 | 16 | |
| | DOCHN | 20 | 13 | |
| Resins | Quinolinohopane | 1 | 2 | |
| | Thioisorenieratane | 2 | 2 | |
| | Benzobisbenzothiophene | 5 | 4 | |
| | Pyridinohopane | 1 | 3 | |
| | Trimethylbenzeneoxane | 15 | 13 | |
| Saturates | Squalane | 3 | 3 | |
| | Hopane | 2 | 2 | |

The four models with increased oxygen were built with 0.5%, 1.0%, 2.0%, and 3.0% more oxygen content than the control binder, resulting in a total oxygen content of 1.4%, 1.9%, 2.9%, and 3.9%, respectively. The range of oxygen content chosen for the models agrees with the range observed in elemental analysis of different aged binders.

To investigate the effect of SARA mass fractions on binder properties, two models in addition to the control virgin binder were built, representing PAV aged binder and RAB binder. These models were built with SARA mass fractions similar to those of PAV aged and RAB binder in Table 3.1, but with no added oxygen to exclude the effect of oxygen content on model properties.

Moreover, two models with SARA mass fractions and oxygen content of PAV aged binder and RAB binder were built to observe the combined effect of both aging mechanisms on binder properties. Figure 3.7 shows a summary of the models used in this study.

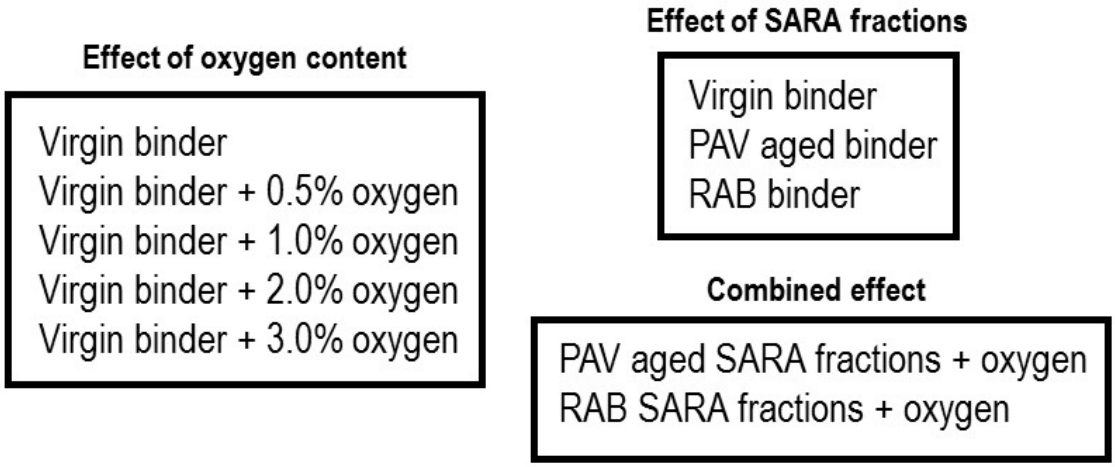


Figure 3.7 A summary of the binder models used in this study

## 3.4 **Molecular dynamics**

Molecular dynamics (MD) simulation determines the trajectory of atoms and molecules in a system by integrating their equation of motion. It solves the classical equation of motion for each atom *i* in a system of *N* atoms which are interacting via a potential *U*. In Cartesian coordinates, the equation of motion is Newton's law of motion:

$$a_i(t) = \frac{dv_i(t)}{dt} = \frac{d^2 r_i(t)}{dt^2} = \frac{F_i}{m_i} \tag{3.1}$$

where $a_i$ is the acceleration of the atom, $v_i$ the velocity of the atom, $t$ is time, $r_i$ is the position of atom, $F_i$ is the force acting on the atom, and $m_i$ is the mass of the atom.

The force $F_i$ is the negative gradient of the potential function $U$:

$$F_i = -\frac{dU_i(r)}{dr_i} \tag{3.2}$$

where $U_i$ is the combination of intramolecular and intermolecular potentials that describe the bonded interactions of the atom within a molecule, as well as nonbonded interactions.

These equations are solved for all atoms at times separated by the time step $\Delta t$. Several algorithms exist for integrating the equation of motion, such as the Verlet algorithm, Velocity Verlet algorithm and leapfrog method. The Velocity Verlet algorithm (Swope et al. 1982), which is a modification of Verlet algorithm, is a popular method for integrating equation of motion in molecular dynamics. In this method, the position and velocity of atom *i* at time *t+dt is* determined using the following equations:

$$r_i(t+dt) = r_i(t) + v_i(t)dt + \frac{1}{2}a_i(t)dt^2 \tag{3.3}$$

$$v_i(t+dt) = v_i(t) + \frac{1}{2}[a_i(t) + a_i(t+dt)]dt \tag{3.4}$$

which are second order Taylor expansions of the equation of motion.

As the name suggests, this method includes the velocity of atoms in the calculation of atom trajectories. This provides an advantage over the basic Verlet equation as molecular dynamic simulations require atom velocities to calculate properties such as temperature and kinetic energy at each time step. This algorithm was used in this study to calculate atom trajectories.

### 3.4.1 Force field

The potential *U* is quantified by the sum of energy terms calculated by empirical functions called valence force fields. These force fields describe the deviation of bond lengths, bond angles, and torsion angles away from equilibrium values. They also include

terms for non-bonded pairs of atoms including van der Waals, electrostatic, and other interactions (Fried 2007). Depending on the force field, different parameters and potential functions are used for each atom type. Due to the wide range of application of molecular dynamic simulations, different force fields have been developed, each with their unique strengths and weaknesses. Notable force fields include DREIDING, OPLS-AA, COMPASS, CHARMM, and AMBER. This study used General AMBER Force Field (GAFF) (Wang et al. 2004) which has been successfully used to simulate asphalt binder in other studies (Khabaz et al. 2015, Yao et al. 2016). General AMBER Force Field is an all-atom force field with the following functional form:

$$E_{\text{pair}} = \sum_{\text{bonds}} k_r(r - r_{\text{eq}})^2 + \sum_{\text{angles}} k_\theta(\theta - \theta_{\text{eq}})^2 + \sum_{\text{dihedrals}} \frac{v_n}{2}[1 + \cos(n\phi - \gamma)] \quad (3.5)$$

$$+ \sum_{i<j} \left[ \frac{A_{ij}}{R_{ij}^{12}} - \frac{B_{ij}}{R_{ij}^{6}} + \frac{q_i q_j}{\varepsilon R_{ij}} \right]$$

where $r_{eq}$ and $\theta_{\text{eq}}$ are equilibrium bond length and angle between two bonds, respectively; $k_r$, $k_\theta$ *and* $V_n$ are force constants for bonds, angles, and dihedrals, respectively; $n$ is multiplicity and $\gamma$ is the phase angle for the torsional angle parameters; The $A$, $B$, and $q$ parameters characterize the nonbonded potentials between particles (Wang et al. 2004).

The first and second terms in the equation are harmonic distance and angle forms, which correspond with bond stretch and bond-angle bend interactions, respectively. The third term is the dihedral angle torsion, which corresponds with the torsional angle between the *ijk* and *jkl* planes formed by the two bonds *ij* and *kl* connected by a common bond *jk*.

The remaining terms calculate the non-bonded interactions between atoms, and include van der Waals and electrostatic interactions. The van der Waals forces are computed by standard 12/6 Lennard Jones potential, which is attractive at large distances and repulsive when the particles are very close together. The electrostatic interactions, which describe the interactions between two charged particles, are computed using Coulomb interaction potential.

### 3.4.2 Ensembles

The thermodynamic state of a system is represented by a small set of parameters, including temperature, volume, pressure, or energy. The microscopic state of a system is defined by atom positions and velocities. An ensemble is a collection of all possible microscopic states of a system that shares similar thermodynamic properties such as temperature and volume. Molecular dynamic simulations are performed under different ensembles, based on the physical situation one intends to model. These ensembles include microcanonical ensemble, canonical ensemble and isothermal-isobaric ensemble, among others. In microcanonical ensemble, NVE, the number of particles (N), volume of the system (V), and total energy of the system (E) is held constant. This is equivalent to a constant volume experiment with no energy exchange with the environment. As the average kinetic energy of particles can vary in this ensemble, the temperature can vary as well. The canonical ensemble, NVT, keeps the number of particles (N), volume of the system (V), and temperature of the system (T) constant. This is equivalent to a constant volume experiment which can exchange heat with the environment. The isothermal-isobaric ensemble, NPT, has constant number of particles (N), system pressure (P), and system temperature (T). This ensemble can be used to simulate a material subject to a

constant pressure, such as atmospheric pressure, that can exchange heat with the surrounding environment.

### 3.4.3 Thermostats and barostats

Constant temperature and pressure conditions in molecular dynamics simulations are enforced using thermostats and barostats. Berendsen, Andersen, and Nose-Hoover algorithms are among the most popular methods used to achieve this goal. In this study, the Nose-Hoover algorithm was used to enforce constant temperature and pressure conditions.

To maintain a constant temperature, this algorithm couples the system with a heat bath, allowing heat to be transferred back and forth between the system and heat bath. To do so, the equation of motion is modified to include an additional term related to the heat bath (Frenkel et al. 2001):

$$a_i(t) = \frac{F_i}{m_i} - \zeta(t)\vec{v}_i(t) \tag{3.6}$$

$$\frac{d}{dt}\zeta(t) = \frac{k_b}{Q}(3NT - (3N+1)T_0) \tag{3.7}$$

where $k_b$ is the Boltzmann constant, $N$ is the number of particles in the system, $T$ is the instantaneous temperature, and $T_0$ is the heat bath temperature. $Q$ is the damping constant, which determines the rate of heat transfer. This parameter should be set carefully, as too large a value will cause the system to take a long time to reach the desired temperature, and too small a value will lead to high temperature fluctuations and simulation instability.

Barostatting using the Nose-Hoover algorithm is achieved by adding dynamic variables to domain dimensions. The pressure damping constant determines how fast the change in domain dimensions occur, and thus should be carefully selected to avoid inefficient barostatting or high pressure fluctuations.

### 3.4.4 Periodic boundary conditions

Periodic boundary conditions are used in molecular dynamic simulations to create bulk state of a material and eliminate edge effects. In a periodic boundary condition model, particles in the simulation box interact not only with other particles in the domain, but with images of particles in neighboring simulation boxes as well. This allows particles to freely cross over the box boundary and enter the adjacent box. When this happens, the image of the same particle will enter the main simulation box from the opposite side, keeping the mass in the box constant and eliminating edge effects. A schematic representation of periodic boundary condition is depicted in Figure 3.8.

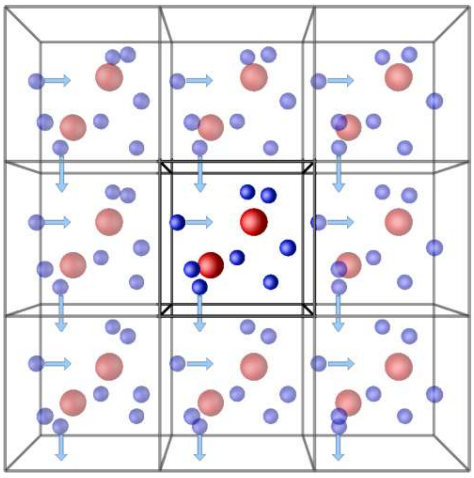

Figure 3.8 Schematic representation of the concept of periodic boundary conditions
From http://isaacs.sourceforge.net/phys/images/these-seb/pbc-seb.png

To avoid interaction between a particle and multiple copies of itself or other particles, the minimum image convention is used with periodic boundary condition. By considering a cut-off radius, defined as the maximum distance up to which a particle interacts with other particles, individual particles in the simulation box can only interact with the closest image of the remining particles in the system. The cut off radius should be smaller than half of any box dimensions to guarantee that each particle cannot interact with two copies of another particle.

## 3.5 **Processing and simulation properties**

The Avogadro molecular builder was used to generate the topology of all molecules. The Antechamber software package was then used for atom and bond type detection as well as partial charge generation according to AM1-bcc method. Partial charges are inputs used by the Columbic potential to model long range electrostatic interactions. The LEap program was used to generate AMBER input files based on the GAFF force field, which were then converted to LAMMPS input files using in-house codes. All molecules were initially put into a large periodic simulation box to avoid overlapping, and then subjected to 100 atmosphere pressure to shrink the simulation box and reach a condensed state. All molecular dynamic simulations were performed using LAMMPS high performance parallel molecular dynamics software. The simulations were performed on high performance computing resources located at University of Nebraska-Lincoln. The number of tasks used to perform each simulation depended on factors such as length of the simulation and number of atoms, and ranged from 50 to 400. Different MATLAB scripts were developed to calculate the desired properties based on software outputs.

Time step selection in molecular dynamic simulations is a compromise between simulation accuracy and computing costs, which are closer to macroscale experiments. Too large a time step can lead to unstable simulations, with total energy of the system increasing rapidly. Time steps ranging from 0.5 to 1 femtoseconds are considered appropriate for all-atom force fields such as GAFF. This study used a time step of 1 fs to achieve longer simulation times, as time steps of 0.7 fs and 0.5 fs were not seen to have any difference on simulation results.

A cutoff radius of 9 angstroms were selected for nonbonded Lennard Jones interactions, which is less than half of the final box length, close to 40 angstroms. The value of cut off radius agrees with the range used in literature, and was not seen to lead to different density values compared to those of a 15-angstrom radius.

## 3.6 **Bulk modulus calculation**

Bulk modulus is a measure of a material's resistance to uniform compression, and is defined as the ratio of an infinitesimal pressure increase to the relative decrease in volume. In this study, bulk modulus of the models was calculated via the method proposed by Tildesley and Allen's (1989), which uses volume fluctuations of the simulation to calculate bulk modulus:

$$K = -V\left(\frac{\partial P}{\partial V}\right)_T = \frac{< V > k_B T}{\left(< V^2 > - < V >^2\right)} \tag{3.8}$$

where $P$ is system pressure, $V$ is system volume, $k_B$ is the Boltzmann constant, $T$ is system temperature, and the brackets denote the time average of the quantity over the duration of the simulation. Bulk modulus simulations were conducted under NPT ensemble for 150 nanoseconds, with a system pressure of 1 atmosphere and temperature

of 135 ºC. This temperature was chosen because the bulk modulus values of simulations at room temperature were found to be highly dependent on the portion of simulation in which the time average was performed. Simulations as long as 200 nanoseconds did not lead to stable results, and thus temperatures above the glass transition temperature of the systems were chosen for bulk modulus calculation.

## 3.7 Glass transition temperature calculation

Glass transition of amorphous materials is a change in which the material moves from a viscous or rubbery state to a hard and relatively brittle glassy state, or vice versa. It occurs when the characteristic time of molecular motions responsible for structural rearrangements becomes longer than the timescale of the experiment. The transition to a glassy state is accompanied by a sudden change in the mechanical and thermodynamic properties of the material, such as an enormous increase in viscosity. The glass transition temperature $T_g$ is the temperature arbitrarily chosen to represent the temperature range over which the glass transition takes place; it is usually assigned to the temperature where half of the sample is already vitrified or devitrified (Kriz 2008).

Given the fact that glass transition is one of the most important factors determining the viscoelastic properties of amorphous materials, this study aimed to investigate the effect of asphalt aging on the glass transition temperature. To do so, three replicates of all models were initially heated up to a temperature of 600 °K, and then subjected to a stepwise cooling at a rate of 10 °K per 2 nanoseconds, until a low temperature of 80 °K was reached. The specific volume of the system at each cooling step was determined by average the values over the second half of the 2-nanosecond simulation. Figure 3.9 shows

the specific volume of the system as a function of temperature for a replicate of the virgin binder model. The glass transition temperature $T_g$ is determined by finding the intersection of tangents in the rubbery and glassy regions of the volume-temperature curve.

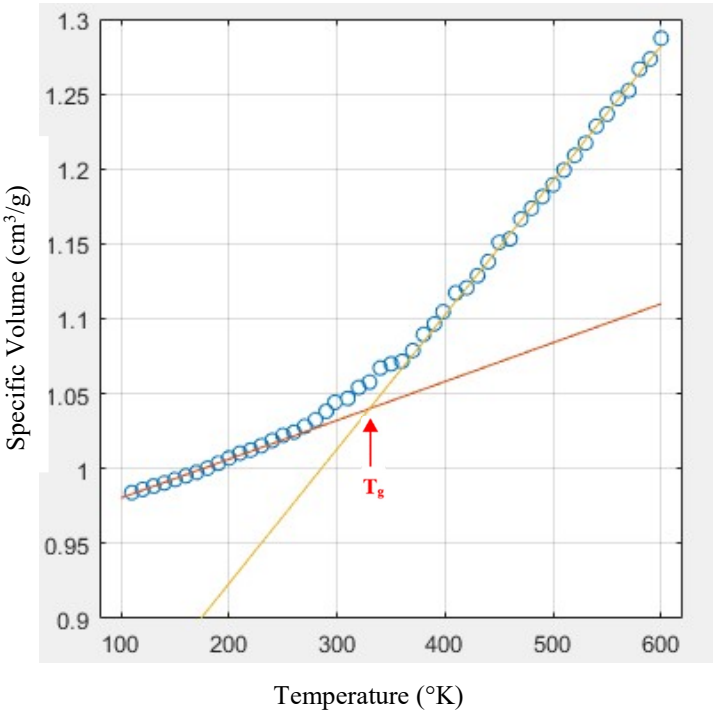


Figure 3.9 Glass transition temperature determination

## 3.8 **Viscosity calculation**

Viscosity of the asphalt models is calculated by deforming the simulation box with a constant strain rate, and measuring the resultant resistant stress in the direction of the shear. As the simulation is not allowed to reach an equilibrium state under constant shear, this method uses non-equilibrium molecular dynamics (NEMD) to calculate viscosity. The simulations were conducted under NVT ensemble for 20 nanoseconds, and at a temperature of 135 °C. Figure 3.10 shows the simulation box in initial and deformed conditions.

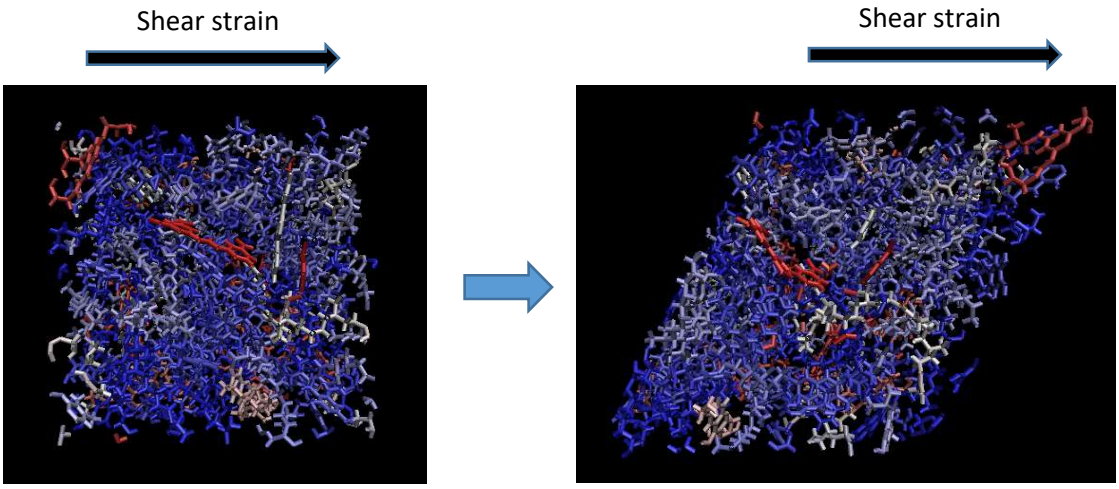


Figure 3.10 Simulation box at initial and sheared conditions during viscosity simualtions

Three different shear rates were used to deform the box, namely $10^{10}$, $10^{9}$ and $10^{8}$ $s^{-1}$. Although lower shear rates will provide viscosity values that are closer to macroscale viscosity test results, at shear rates lower than $10^{8}$ $s^{-1}$ the velocity profile of molecules as a function of height no longer follows a linear trend. This indicates that the random movement of the molecules have a larger magnitude than the induced shear strain, which leads to inaccurate viscosity values. Therefore, shear rates lower than $10^{8}$ $s^{-1}$ were not considered in this study. To observe the effect of shear plane on viscosity values, simulations with shear in both *xy* and *xz* planes were conducted. The calculated values had less than 2% difference, indicating that the viscosity measurement is independent of the shear plane. Therefore, shear in *xy* plane was used to calculate the viscosity in all models in this study. Similarly, two models were built with two and three times the number of molecules in virgin binder model, to investigate the effect of model size on viscosity values. Comparison of results with the smaller virgin binder model showed less than 4% difference in viscosity values, indicating that the smaller size of model provides satisfactory accuracy.

# CHAPTER 4
# RESULTS AND DISCUSSION

## 4.1 Density

The average density results of different models after equilibrium conditions is shown in Figures 4.1 and 4.2. Increase in oxygen content of binder led to a steady increase in density of the system, which can be explained by the increase in intermolecular interactions due to presence of polar molecules. The SARA fractions of PAV aged and RAB binder both led to an increase in density of binder. This can be attributed to the presence of higher fractions of denser molecules within the binder. The density of RAB binder with oxygen is higher than the density of PAV binder with oxygen, as the increase in density is more significant with increase in oxygen content.

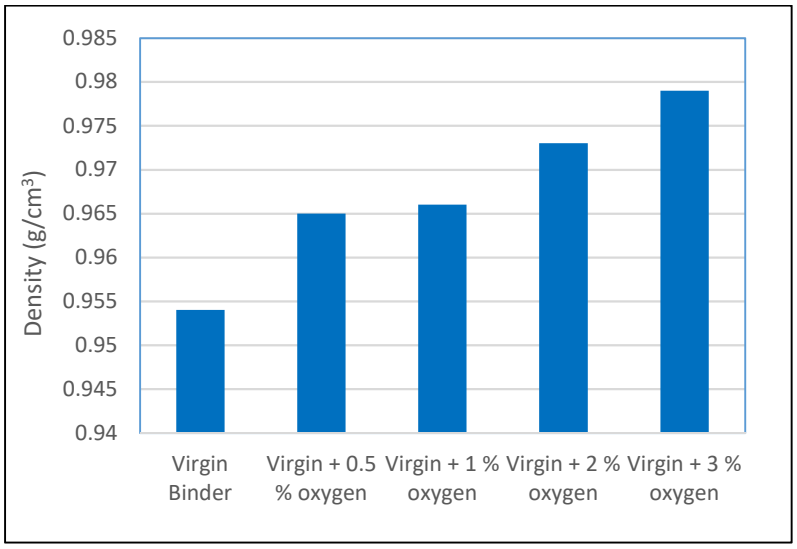


Figure 4.1 Density results for models with different oxygen content

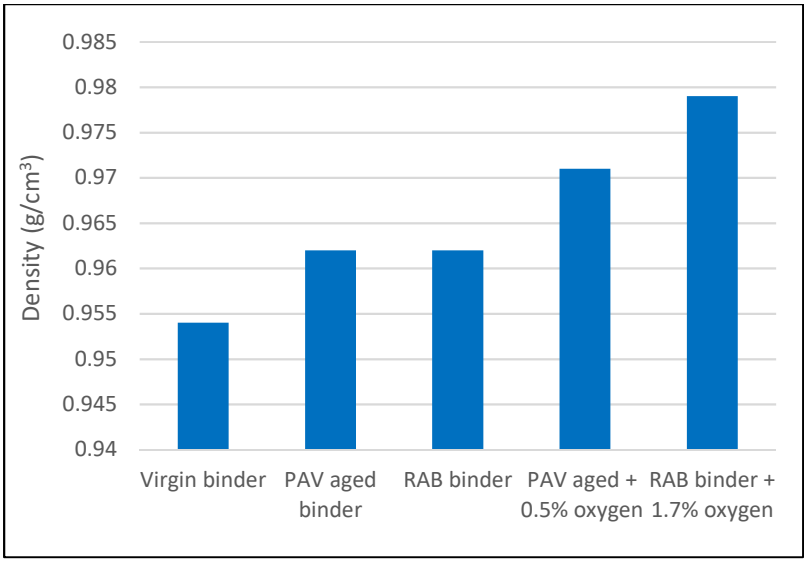


Figure 4.2 Density results for different SARA fractions and combined models

## 4.2 **Bulk modulus results**

The bulk modulus results for different models is shown in Figure 4.3. All oxidized models show higher bulk modulus values compared to the virgin binder model, with increasing values for higher oxygen content. The SARA fractions of aged binder lead to an increase in bulk modulus as well, with RAB binder model showing a higher value compared to virgin binder, but lower value compared to PAV aged binder. For the combined models with added oxygen, PAV aged binder shows less difference compared to RAB binder, indicating that the oxygen content of RAB binder had a larger effect on its bulk modulus value, compared to PAV aged binder.

The results obtained by increasing oxygen content and changing the SARA fractions are both in a good agreement with the stiffening effect of asphalt due to aging, and can be attributed to the stronger inter-molecular interactions and higher portions of densely packed molecules.

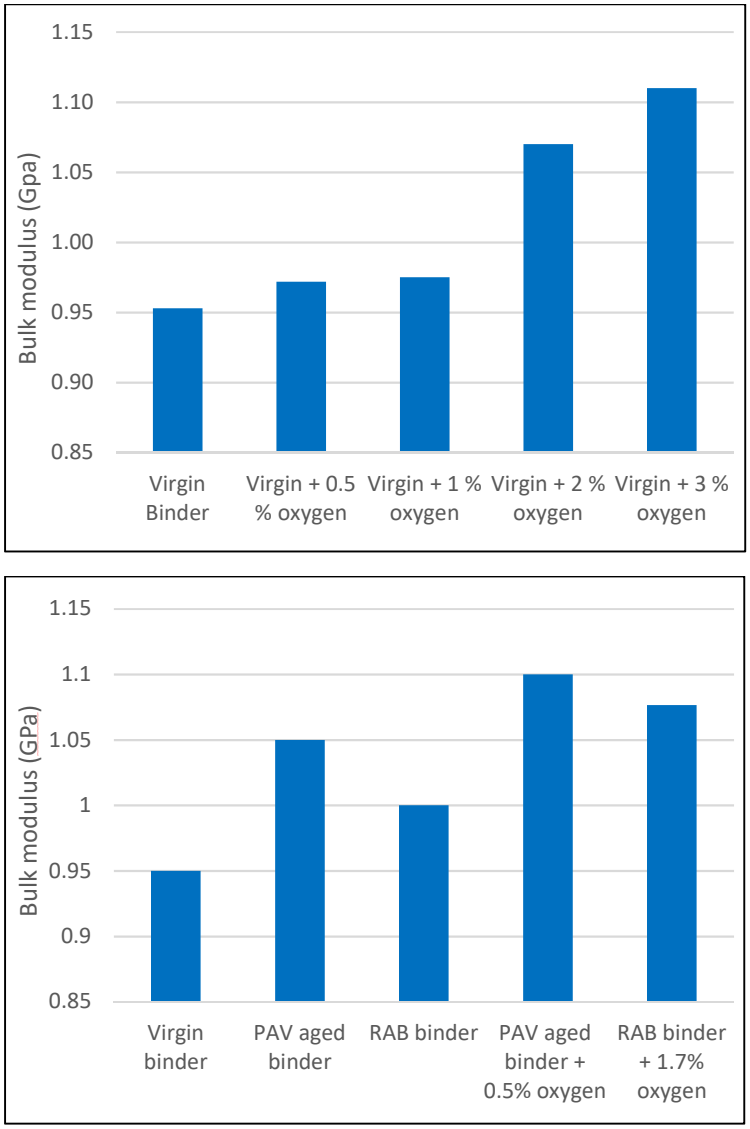


Figure 4.3 Bulk modulus results for different models

## 4.3 **Glass transition temperature results**

The glass transition temperature was obtained by determining the point in specific volume-temperature curve where the change in slope occurs. Figure 4.4 shows the glass transition results for different models. The error bars show that the glass transition temperature of the system varies considerably for different replicates, and depends on the initial state of the simulation. The glass transition temperature of virgin binder appeared

to be lower than all other models, but no relationship is observed between increased oxygen content or change in SARA fractions, and glass transition temperature of the system.

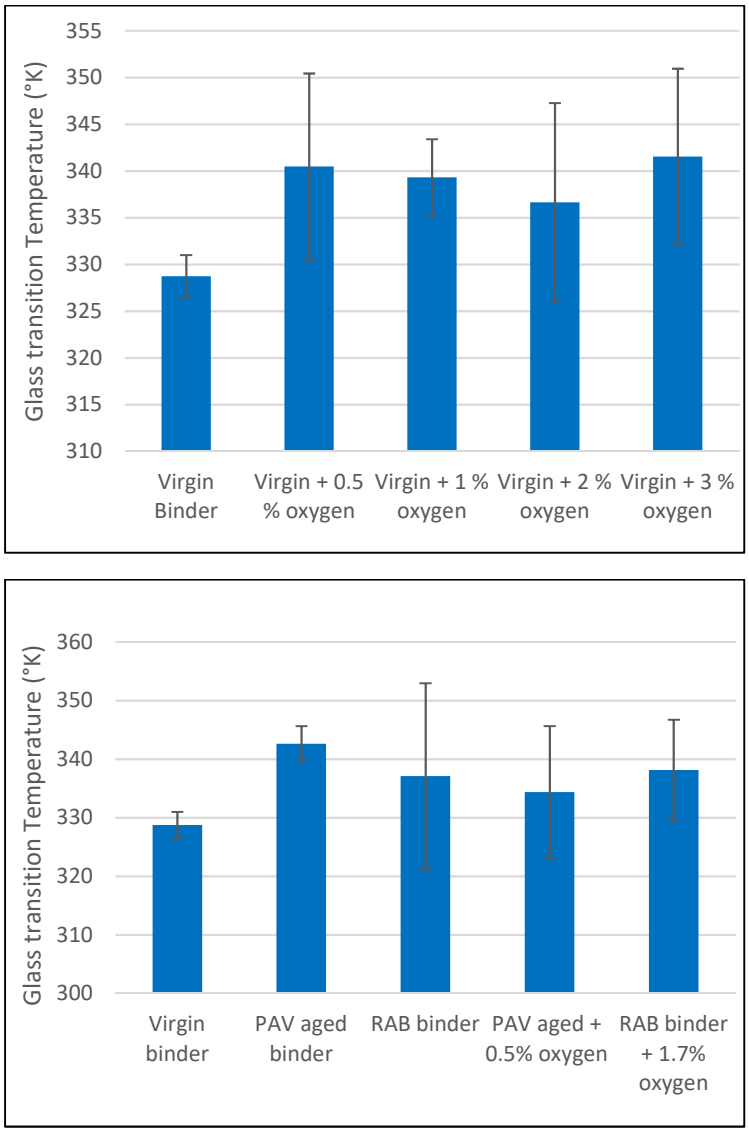


Figure 4.4 Glass transition temperature for different models

The glass transition temperatures obtained using simulations is in the range of 52 °C to 82 °C which is much higher than the values obtained using macroscale measurements. This is due to the high cooling rate used in the MD simulation, which is a well-known factor affecting the glass transition temperature value (Khabaz and Khare 2015).

Dynamic mechanical analysis of virgin and lab aged binder has shown that glass transition temperature increases as the binder becomes stiff due to aging (Daly et al. 2010). Such results were also expected in this study, but were not observed. The high dependability of $T_g$ results on the initial state of the system could be the reason. Figure 4.5 shows the specific volume-temperature curve for 3 replicates of the same asphalt model. At high temperatures, the curve and the tangent line are similar for all replicates, as the molecules can easily move and achieve low energy configurations. However, starting at roughly 350 °K, the curves for different replicates start to diverge, leading to different tangent lines at low temperatures and consequently different glass transition temperatures. As the molecules have less mobility at lower temperatures, it takes a longer time for the system to reach a low energy configuration. The fast cooling rate of the simulation does not allow all replicates to reach the same energy level at each temperature, and thus each replicate demonstrates a different specific volume. A lower cooling rate is believed to lead to more consistent results for different replicates, but will be much more computationally expensive. Using a higher number of molecules and therefore a larger simulation box will reduce the fluctuations in calculated properties, but will also be costly in terms of computation time. Higher computational power will allow for larger systems and longer simulation times, and is expected to lead to more consistency in the calculated properties.

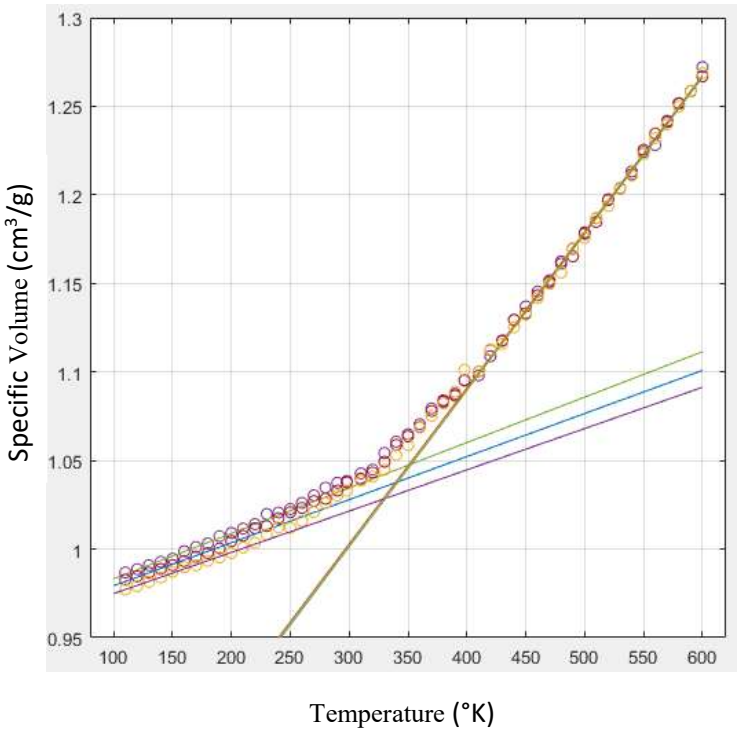


Figure 4.5 Glass transition temperature for three replicates of the same binder model

## Viscosity results

The shear stress value for each shear rate was obtained by time-averaging shear stress over the duration of the simulation. The time-averaged stress value for different parts of the simulation were seen to be in good agreement, indicating stability of the simulation results. Therefore, only one replicate was used for each model and shear rate. The viscosity results for different models and shear rates is shown in Figure 4.6. For all shear rates, oxidized systems show higher viscosity compared to virgin binder, with larger viscosity values for higher oxygen content. This is in agreement with the stiffening observed in macroscale experiments of aged binder. The magnitude of increase in viscosity depends on the shear rate, with $10^{10}$ $s^{-1}$ shear rate showing less than 20% viscosity difference between virgin and the most oxidized model, while at $10^{8}$ $s^{-1}$ shear rate the viscosity increases more than 70%. In the case of different SARA fractions, the

results of all shear rates showed a significant increase in viscosity for PAV aged binder compared to virgin binder, and a slight increase for RAB binder. This can be attributed to the high asphaltene content of PAV aged binder compared to RAB binder. The combined model for PAV aged binder had a slightly higher viscosity value than the combined model for RAB binder. Comparing the combined models with PAV aged and RAB SARA models shows that the increase in viscosity for PAV aged binder occurs mainly due to the upset in the balance of SARA fractions. For RAB binder, however, the oxygen content of the model is the major factor contributing to the high viscosity value. Therefore, although PAV aging increases the viscosity similar to field aging, the underlying mechanism leading to the increase in viscosity is not similar for these aging types.

Rejuvenators are mainly used to increase the fractions of lighter molecules and restore the balance in SARA fractions of aged binder. Therefore, for PAV aged binder, rejuvenators are expected to directly counter the effect of aging, as the main aging mechanism is the upset in SARA fractions. In the case of field aged binder, however, the main aging mechanism is oxidation. Although adding rejuvenators can restore ductility to the binder, it does not counter the effect of oxidation. Instead, it modifies the balance in fractions to compensate for the ductility lost due to oxidation.

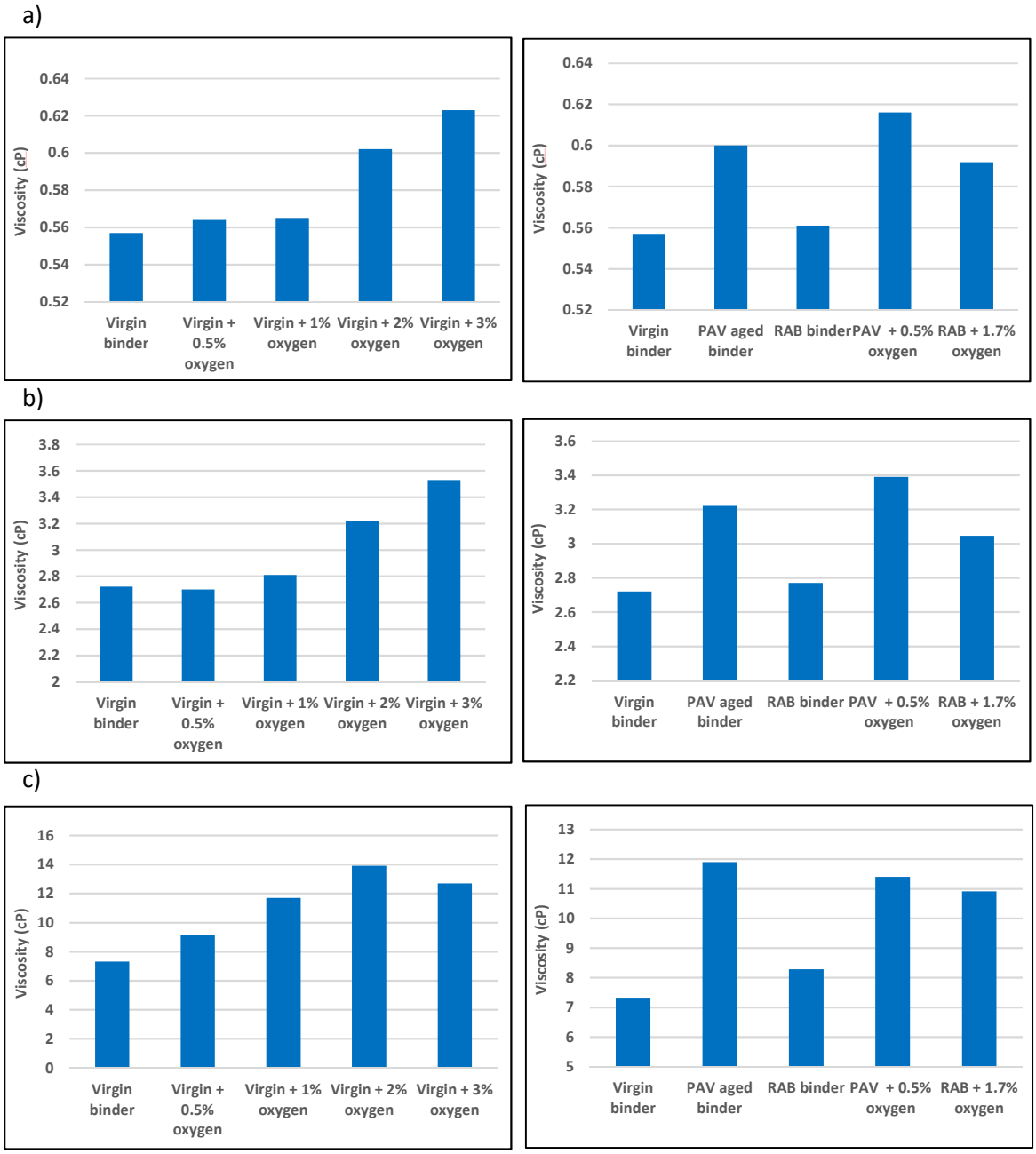


Figure 4.6 Viscosity values for different models at a) $10^{10}$, b) $10^{9}$, and c) $10^{8}$ $s^{-1}$ shear rates

The decreasing viscosity values for higher shear rates indicates that asphalt binder demonstrates a shear-thinning behavior at high shear rates. The shear rates used in the simulation were much higher than the shear rates in typical macroscale experiments, and therefore lower shear rates should be used if an accurate prediction of macroscale properties is intended. However, at lower shear rates, the random movement of the molecules becomes more significant than the induced shear movement, and the viscosity results will be highly dependent on the instantaneous state of the system. To achieve accurate viscosity predictions, one should simulate the shear for such a large duration that the time-average of properties starts to converge, and the system fluctuations balance each other. This, however, calls for longer simulation durations and higher computational power, and is outside the scope of this research.

# CHAPTER 5
# CONCLUSION AND RECOMMENDATION

## 5.1 Summary and conclusion

In this thesis, the effect of oxygen content and SARA fractions on the behavior of asphalt binder was studied using MD simulation. Different asphalt models were built and their properties were compared, illustrating how each aging mechanism affected asphalt properties. This study provides more insight into the fundamentals of asphalt aging, showing how factors at the molecular scale affect the macroscale properties of binder. Understanding the link between length-scales can enable the manufacturing of binders with desirable characteristics, such as improved aging resistance. Moreover, MD modeling can be used to predict the properties of asphalt when subjected to chemical changes such as aging or addition of rejuvenators.

The following conclusions are drawn from the results of this study:

- The density of asphalt increased with increased oxygen content and for aged binder SARA fractions. The density increase for oxidized asphalt can be attributed to the presence of more polar molecules and stronger intermolecular interactions. The density increase for aged binder SARA fractions can be explained by the increased content of densely packed molecules i.e. asphaltenes.
- The bulk modulus of asphalt increased with oxidation and for SARA fractions of aged binder. The SARA fractions of PAV aged binder led to a higher bulk modulus compared to RAB binder, indicating that the change in SARA fractions

during PAV aging causes more stiffening compared to field aging. The combined model for PAV aged binder had a slightly higher bulk modulus than RAB binder.

- No statistically significant difference was observed between glass transition temperatures of virgin and aged binder models. The tangents of the specific volume-temperature curve in the rubbery region of models were similar for different replicates of the same model. However, the tangents in the glassy region were different, leading to different $T_g$ values for each replicate. It is possible that a slower cooling rate will allow the molecules to reach a lower energy state at low temperatures, resulting in more consistent $T_g$ values.
- Increased oxygen content of the system and the SARA fractions of aged binder both led to an increase in binder viscosity. The viscosity of the model with SARA fractions from PAV aged binder was significantly higher than the viscosity of virgin binder and the model with RAB SARA fractions. When the oxygen content of models was considered, RAB binder showed significantly higher viscosity compared to virgin binder, but still lower viscosity compared to PAV aged binder. This indicates that the dominant mechanism affecting the viscosity is different for laboratory and field aging.
- Rejuvenating agents are aimed at restoring the balance of SARA fractions and are not usually capable of reversing oxidation in asphalt. Thus, rejuvenating PAV aged binder is expected to directly counter the aging mechanism when restoring binder ductility, as PAV aging alters the balance of SARA fractions more dramatically. For field aged binder, however, the main aging mechanism seems oxidation. Although rejuvenation restores the properties of binder, it does so by

mostly changing the SARA fractions and compensating for the ductility lost due to oxidation.

## 5.2 Recommendation for further study

- The asphalt models used in this study, despite being an improvement over previous models, can still be further improved to obtain a more realistic representation of bitumen. Specifically, the low number of heteroatoms in the model did not allow making of models with realistic sulfur and nitrogen content. As the number of molecular dynamic studies on asphalt properties is increasing, a more realistic model of bitumen will certainly prove valuable to the asphalt research community.
- The computational power available for performing the simulations limited the duration of simulation to one or two hundred nanoseconds. Longer simulations times will ensure that the system goes through different possible states. Using more powerful computer resources will make the properties better representing real material behavior.
- Although some theories exist regarding how SARA fractions change and transform during aging, the mechanism is not fully understood. More studies on the chemical reactions that lead to higher asphaltene content and lower maltene content can provide valuable information on asphalt aging.
- This study did not investigate the effect of aging on other asphalt properties such as intrinsic healing ability, moisture susceptibility, shear modulus, adhesion strength, etc. Calculation of each of these properties for different models of aged binder will provide more insights into how aging affects properties of binder.

- Only ketone and sulfoxide functional groups were used in this study to simulate oxidation of asphalt molecules. Although these functional groups are the main products of oxidation, inclusion of other oxidation products will lead to a more realistic representation of actual oxidation.
- The effect of various kinds of rejuvenators can be investigated on aged binder performance. Rejuvenators will likely be able to reverse the change in properties due to the upset in SARA fractions. It is unlikely, however, that they can mitigate the effect of oxidation within asphalt. A molecular dynamic study of rejuvenated asphalt binder will provide interesting information regarding the effectiveness of different types of rejuvenator.

# REFERENCES

Artok, Levent, Yan Su, Yoshihisa Hirose, Masahiro Hosokawa, Satoru Murata, and Masakatsu Nomura. "Structure and reactivity of petroleum-derived asphaltene." *Energy & Fuels* 13, no. 2 (1999): 287-296.

Allen, Mike P., and Dominic J. Tildesley. Computer simulation of liquids. Oxford university press, 1989.

Bell, Chris A. *Summary report on aging of asphalt-aggregate systems*. No. SHRP-A-305. 1989.

Bhasin, Amit, Rammohan Bommavaram, Michael L. Greenfield, and Dallas N. Little. "Use of molecular dynamics to investigate self-healing mechanisms in asphalt binders." *Journal of Materials in Civil Engineering* 23, no. 4 (2010): 485-492.

Boysen, R. and J. Schabron, *Laboratory and Field Asphalt Binder Aging: Chemical Changes and Influence on Asphalt Binder Embrittlement.* Federal Highway Administration, Report No. FHWA-HRT-11-045, McLean, VA, 2015.

Branthaver, Jan Franklin, J. C. Petersen, R. E. Robertson, J. J. Duvall, S. S. Kim, P. M. Harnsberger, T. Mill, E. K. Ensley, F. A. Barbour, and J. F. Scharbron. *Binder characterization and evaluation. Volume 2: Chemistry*. No. SHRP-A-368. 1993.

Claudy, P., Letoffe, J. M., King, G. N., and Plancke, J. P. (1992). “Characterization of Asphalts Cements by Thermomicroscopy and Differential Scanning Calorimetry: Correlation to Classic Physical Properties.” *Fuel Science and Technology International*, Taylor & Francis, 10(4-6), 735–765.

Corbett, Luke W. "Composition of asphalt based on generic fractionation, using solvent deasphaltening, elution-adsorption chromatography, and densimetric characterization." Analytical Chemistry 41, no. 4 (1969): 576-579.

Cornell, Wendy D., Piotr Cieplak, Christopher I. Bayly, Ian R. Gould, Kenneth M. Merz, David M. Ferguson, David C. Spellmeyer, Thomas Fox, James W. Caldwell, and Peter A. Kollman. "A second generation force field for the simulation of proteins, nucleic acids,

and organic molecules." *Journal of the American Chemical Society* 117, no. 19 (1995): 5179-5197.

Daly, William H., Ioan I. Negulescu, and Ionela Glover. "A comparative analysis of modified binders: original asphalts and materials extracted from existing pavements." *Federal Highway Administration Report No. FHWA/LA* 10 (2010): 462

Ding, Yongjie, Boming Tang, Yuzhen Zhang, Jianming Wei, and Xuejuan Cao. "Molecular Dynamics Simulation to Investigate the Influence of SBS on Molecular Agglomeration Behavior of Asphalt." *Journal of Materials in Civil Engineering* 27, no. 8 (2013): C4014004.

Ding, Yongjie, Baoshan Huang, Xiang Shu, Yuzhen Zhang, and Mark E. Woods. "Use of molecular dynamics to investigate diffusion between virgin and aged asphalt binders." *Fuel* 174 (2016): 267-273.

Frenkel, Daan, and Berend Smit. *Understanding molecular simulation: from algorithms to applications*. Vol. 1. Academic press, 2001.

Fried, J. R. (2007). “Chapter 4 Computational Parameters.” *Physical Properties of Polymers Handbook*, J. E. Mark, ed., Springer, New York, NY, 59–65.

Greenfield, Michael L. "Molecular modelling and simulation of asphaltenes and bituminous materials." *International Journal of Pavement Engineering* 12, no. 4 (2011): 325-341.

Groenzin, Henning, and Oliver C. Mullins. "Molecular size and structure of asphaltenes from various sources." *Energy & Fuels* 14, no. 3 (2000): 677-684.

Hansen, Jesper Schmidt, Claire A. Lemarchand, Erik Nielsen, Jeppe C. Dyre, and Thomas Schrøder. "Four-component united-atom model of bitumen." *The Journal of chemical physics* 138, no. 9 (2013): 094508.

Jennings, P. W., J. A. Pribanic, M. A. Desando, M. F. Raub, R. Moats, J. A. Smith, T. M. Mendes et al. *Binder characterization and evaluation by nuclear magnetic resonance spectroscopy*. No. SHRP-A-335. 1993.

Khabaz, Fardin, and Rajesh Khare. "Glass transition and molecular mobility in styrene–butadiene rubber modified asphalt." *The Journal of Physical Chemistry B* 119, no. 44 (2015): 14261-14269.

Kriz, Pavel, Jiri Stastna, and Ludo Zanzotto. "Glass transition and phase stability in asphalt binders." *Road Materials and Pavement Design* 9, no. sup1 (2008): 37-65.

Lemarchand, Claire A., Thomas B. Schrøder, Jeppe C. Dyre, and Jesper S. Hansen. "Cooee bitumen: Chemical aging." *The Journal of chemical physics* 139, no. 12 (2013): 124506.

Lesueur, Didier. "The colloidal structure of bitumen: consequences on the rheology and on the mechanisms of bitumen modification." *Advances in colloid and interface science* 145, no. 1 (2009): 42-82.

Li, Derek D., and Michael L. Greenfield. "Chemical compositions of improved model asphalt systems for molecular simulations." Fuel 115 (2014): 347-356.

Martín-Martínez, Francisco J., Elham H. Fini, and Markus J. Buehler. "Molecular asphaltene models based on Clar sextet theory." RSC Advances 5, no. 1 (2015): 753-759.

Mortazavi, Massoud, and James S. Moulthrop. "The SHRP materials reference library." (1993).

Mullins, Oliver C. "The modified Yen model." *Energy & Fuels* 24, no. 4 (2010): 2179-2207.

Murgich, Juan, Jesús Rodríguez, and Yosslen Aray. "Molecular recognition and molecular mechanics of micelles of some model asphaltenes and resins." *Energy & Fuels* 10, no. 1 (1996): 68-76.

NCAT, *NCAT Researchers Explore Multiple Uses of Rejuvenators*. 2014, National Center for Asphalt Technology. p. 7-9.

Pahlavan, Farideh, Masoumeh Mousavi, Albert Hung, and Ellie H. Fini. "Investigating molecular interactions and surface morphology of wax-doped asphaltenes." *Physical Chemistry Chemical Physics* 18, no. 13 (2016): 8840-8854.

Pan, Tongyan, Yang Lu, and Stephen Lloyd. "Quantum-chemistry study of asphalt oxidative aging: an XPS-aided analysis." Industrial & Engineering Chemistry Research 51, no. 23 (2012a): 7957-7966.

Pan ,Tongyan, Yang Lu, and Zhaoyang Wang. "Development of an atomistic-based chemophysical environment for modelling asphalt oxidation." Polymer degradation and stability 97, no. 11 (2012b): 2331-2339.

Pan, Jielin, and Rafiqul A. Tarefder. "Investigation of asphalt aging behaviour due to oxidation using molecular dynamics simulation." *Molecular Simulation* 42, no. 8 (2016): 667-678.

Petersen, J. C., F. A. Barbour, and S. M. Dorrence. Catalysis of Asphalt Oxidation by Mineral Aggregate Surfaces and Asphalt Components. Proc., Association of Asphalt Paving Technologists, Vol. 43, 1974, pp. 162–177

Petersen, J. C. "Chemical Composition of Asphalt as Related to Asphalt Durability: State of the Art." Transportation Research Record 999: 13 (1984).

Petersen, J. Claine. "Quantitative functional group analysis of asphalts using differential infrared spectrometry and selective chemical reactions--theory and application." Transportation Research Record 1096 (1986).

Petersen, J. C., R. E. Robertson, J. F. Branthaver, P. M. Harnsberger, J. J. Duvall, S. S. Kim, D. A. Anderson, D. W. Christiansen, and H. U. Bahia. "Binder characterization and evaluation: Volume 1." *Rep. No. SHRP-A-367, Strategic Highway Research Program, National Research Council, Washington, DC., Google Scholar* (1994).

Petersen, J. Claine. "A review of the fundamentals of asphalt oxidation: chemical, physicochemical, physical property, and durability relationships." *Transportation Research E-Circular* E-C140 (2009).

Petersen, J. Claine, and Ronald Glaser. "Asphalt oxidation mechanisms and the role of oxidation products on age hardening revisited." Road Materials and Pavement Design 12, no. 4 (2011): 795-819.

Qin, Q., J.F. Schabron, R.B. Boysen, and M.J. Farrar, Field aging effect on chemistry and rheology of asphalt binders and rheological predictions for field aging. Fuel, 2014. 121: p. 86-94.

Read, John, and David Whiteoak. *The shell bitumen handbook*. Thomas Telford, 2003.

Robertson RE. *Chemical properties of asphalts and their relationship to pavement performanc*e. In: Strategic highway research program. Washington, DC, USA: National Research Council; 1991.

Rogel, E., and L. Carbognani. "Density estimation of asphaltenes using molecular dynamics simulations." *Energy & fuels* 17, no. 2 (2003): 378-386.

Siskin, M., S. R. Kelemen, C. P. Eppig, L. D. Brown, and M. Afeworki. "Asphaltene molecular structure and chemical influences on the morphology of coke produced in delayed coking." *Energy & Fuels* 20, no. 3 (2006): 1227-1234.

Sun, Daquan, Tianban Lin, Xingyi Zhu, Yang Tian, and Fuliang Liu. "Indices for self-healing performance assessments based on molecular dynamics simulation of asphalt binders." *Computational Materials Science* 114 (2016): 86-93.

Swope, William C., Hans C. Andersen, Peter H. Berens, and Kent R. Wilson. "A computer simulation method for the calculation of equilibrium constants for the formation of physical clusters of molecules: Application to small water clusters." *The Journal of Chemical Physics* 76, no. 1 (1982): 637-649.

Takanohashi, Toshimasa, Shinya Sato, Ikuo Saito, and Ryuzo Tanaka. "Molecular dynamics simulation of the heat-induced relaxation of asphaltene aggregates." *Energy & fuels* 17, no. 1 (2003): 135-139.

Wang, Hao, Enqiang Lin, and Guangji Xu. "Molecular dynamics simulation of asphalt-aggregate interface adhesion strength with moisture effect." *International Journal of Pavement Engineering* 18, no. 5 (2017): 414-423.

Wang, Junmei, Romain M. Wolf, James W. Caldwell, Peter A. Kollman, and David A. Case. "Development and testing of a general amber force field." *Journal of computational chemistry* 25, no. 9 (2004): 1157-1174.

Wiehe, I. A., and K. S. Liang. "Asphaltenes, resins, and other petroleum macromolecules." Fluid Phase Equilibria 117, no. 1 (1996): 201-210.

Verlet, Loup. "Computer" experiments" on classical fluids. I. Thermodynamical properties of Lennard-Jones molecules." *Physical review* 159, no. 1 (1967): 98.

Xu, Guangji, and Hao Wang. "Study of cohesion and adhesion properties of asphalt concrete with molecular dynamics simulation." *Computational Materials Science* 112 (2016): 161-169.

Xu, Guangji, and Hao Wang. "Molecular dynamics study of oxidative aging effect on asphalt binder properties." *Fuel* 188 (2017): 1-10.

Xu, Meng, Junyan Yi, Decheng Feng, Yudong Huang, and Dongsheng Wang. "Analysis of Adhesive Characteristics of Asphalt Based on Atomic Force Microscopy and Molecular Dynamics Simulation." *ACS applied materials & interfaces* 8, no. 19 (2016): 12393-12403.

Yao, Hui, Qingli Dai, and Zhanping You. "Chemo-physical analysis and molecular dynamics (MD) simulation of moisture susceptibility of nano hydrated lime modified asphalt mixtures." *Construction and Building Materials* 101 (2015): 536-547.

Yao, Hui, Qingli Dai, and Zhanping You. "Molecular dynamics simulation of physicochemical properties of the asphalt model." *Fuel* 164 (2016): 83-93.

Zhang, Liqun, and Michael L. Greenfield. "Analyzing properties of model asphalts using molecular simulation." Energy & fuels 21, no. 3 (2007): 1712-1716.